UNIVERSITY OF CALIFORNIA,
IRVINE

Gold Nanowire Thermophones

THESIS

submitted in partial satisfaction of the requirements
for the degree of

MASTER OF SCIENCE

in Chemical and Materials Physics

by

Rajen Kumar Dutta

Thesis Committee:
Professor Reginald M. Penner, Chair
Professor Zuzanna S. Siwy
Professor Shane Ardo

2016

DEDICATION

To my friends and family who have supported me every step of the way.
-RKD

TABLE OF CONTENTS

LIST OF FIGURES

LIST OF TABLES

ACKNOWLEDGMENTS

I would like to thank Brian Albee, Dr. Wytze E. van der Veer, Taylor Harville, Dr. Keith C. Donavan, Professor Dimitri Papamoschou, and Professor Reginald M. Penner for their support and assistance in this study. I gratefully acknowledge the financial support of this work by the National Science Foundation Division of Chemistry through Contract CHE-1306928. Electron microscopy was performed at the LEXI facility at UCI and microphone measurements were collected at the Aeroacoustics Lab at UCI.

Adapted with permission from Dutta, Rajen, et al. "Gold Nanowire Thermophones." The Journal of Physical Chemistry C 118.50 (2014): 29101-29107.

ABSTRACT OF THE THESIS

Gold Nanowire Thermophones

By

Rajen Kumar Dutta

Master of Science in Chemical and Materials Physics

University of California, Irvine, 2016

Professor Reginald M. Penner, Chair

Ultra-long (mm scale) polycrystalline gold nanowires were investigated for their ability to perform as thermophones, or thermoacoustic sound emitters. Arrays of ∼4000 linear gold nanowires are fabricated at 5μm pitch on glass surfaces using lithographically patterned nanowire electrodeposition (LPNE). The properties of nanowire arrays for generating sound are evaluated as a function of frequency (from 5 - 120 kHz), angle from the plane of the nanowires, input power (from 0.30 - 2.5 W) and the width of the nanowires in the array (from 270 to 500 nm.) Classical theory for thermophones based upon metal films accurately predicts the measured properties of these gold nanowire arrays. Angular "nodes" for the off-axis sound pressure level (SPL) versus frequency data, predicted by the directivity factor, are faithfully reproduced by these nanowire arrays. The maximum efficiency of these arrays ($\sim 10^{-10}$ at 25 kHz), the power dependence, and the frequency dependence is independent of the lateral dimensions of these wires over the range from 270 to 500 nm.

Chapter 1

Introduction

Thermoacoustic speakers, also called thermophones, are transducers consisting of a low heat capacity conductor, such as a metal film. The application of an alternating current (ac) at a frequency ω to this conductor induces Joule heating of the conductor at a frequency 2ω. The resulting heat flux into the contacting air layer causes pressure oscillations that radiate as sound away from the conductor, also at a frequency of 2ω. Thus, thermophones are loudspeakers with no moving parts, and no magnets.

Arnold and Crandall[1] published a seminal paper on thermophones in 1917 that described many of the unique properties of these devices but in the nearly one hundred years since, interest in thermophones has waned. Then in 2008, Xiao *et al.*[16] demonstrated that free-standing films of carbon nanotubes (CNTs) could function as thermophones and be transparent, flexible, and stretchable.[16] This work directed attention towards other types of

Table 1.1: Literature Summary of Thermophone Devices and Performance Metrics

Conductor[a]	Architecture	Substrate[a]	Efficiency	Ref
Al	suspended nanowire array	Si/air gap	3×10^{-6}	[12]
Pt	suspended film	–	nr	[1]
CNT	suspended film	–	nr	[16]
Al	film	porous Si	9×10^{-8}	[7]
CNT	suspended bundles	Si	nr	[13]
ITO	film	glass	6.3×10^{-8}	[11]
Graphene	film	paper	1×10^{-6}	[8]
PEDOT	film	glass	1.9×10^{-5}	[9]
Ag	nanowire mesh film	PET	2.1×10^{-5}	[10]
Au	**nanowire array**	**glass**	$\mathbf{1.9 \times 10^{-10}}$	**This work**

[a]Abbreviations: CNT = carbon nanotube, ITO - indium tin oxide-coated glass, PEDOT = poly(3,4-ethylenedioxythiophene), PET = polyethylene terephthalate, nr = not reported

nanomaterials capable of functioning as thermoacoustic transducers. Niskanen and Vesterinen *et al.*[6, 12] fabricated arrays of aluminum ribbons, 3 μm (w) $\times$ 30 nm (h), that were suspended across 200 μm trenches on a silicon surface. These devices produced frequency-dependent sound pressure levels in accord with theory and showed a maximum efficiency for sound generation of 3×10^{-6} at $\sim$40 kHz.[12] Tian *et al.*[10] investigated the properties of films of thermally annealed silver nanowires randomly distributed on glass and polyethylene terephthalate (PET) surfaces. The individual silver nanowires in these films were 80-240 nm in diameter and 15 μm, on average, in length. Efficiencies of up to 10^{-5} were obtained at 10-20 kHz.[10] Finally, Wei *et al.*[13] fabricated thermophones from arrays of carbon nanotube "yarns" that were $\sim$30 μm in diameter and suspended across 600 μm grooves on a silicon substrate. The efficiency of this system was not reported, however.[13] All other recent work of which we are aware (Table 1.1) has involved an evaluation of optically transparent films composed of metals,[7] graphene,[8] indium tin oxide (ITO)-coated glass,[11] and the electronically conductive polymer PEDOT (poly(3,4-ethylenedioxythiophene)).[9]

The objective of our work was to characterize the properties of ultra-long (mm scale) polycrystalline gold nanowires as thermophones. Arrays of ∼4000 linear, gold nanowires have been fabricated at 5 μm pitch on glass surfaces using lithographically patterned nanowire electrodeposition (LPNE).[5, 14, 15] As compared with films of silver nanowires investigated by Tian *et al.*[10], these gold nanowire arrays have precisely defined lateral dimensions and nanowire-nanowire junctions are not present within the array. Such precisely defined gold nanowire arrays therefore afford an opportunity to quantitatively compare experimentally measured performance with the predictions of theory. The wire height in this study was maintained at a value of 100(±8) nm and a range of wire widths was explored, ranging from 270(±14) to 500(±28) nm. We found that classical theory for thermophones is remarkably accurate in predicting the behavior of gold nanowire arrays. Angular "nodes" for the off-axis sound pressure level (SPL) versus frequency data, predicted by the directivity factor, are faithfully reproduced by these nanowire arrays. But the maximum efficiency of these arrays is low ($\sim 10^{-10}$ at 25 kHz) and independent of the wire width over the range of explored here.

Chapter 2

Experimental Methods

2.1 Chemicals and Materials

Positive photoresist Shipley S-1808 and developer MF-319 were purchased from Microchem Corporation. Nickel wire (4 N purity, ESPI Metals), gold pellets (5 N purity, Kurt J. Lesker Co.) and chromium powder (3 N purity, American Elements) were used for the evaporation of films.

2.2 Fabrication of Gold Nanowire Thermophones

Nanowire thermophone devices were fabricated using LPNE [5, 14, 15], as depicted in Figure 2.1. Starting with a clean soda lime glass slide, a 100 nm thick layer of nickel was thermally evaporated onto the surface (1). A layer of photoresist (PR) was then spin-coated onto the surface (2) and baked in a 90°C oven for 30 minutes. Using a contact mask with a 365 nm UV light source, shutter, and alignment stage (Newport, 83210i-line, 1.80s), the photoresist layer was patterned, then developed (3) for 30 s (Shipley, MF-319) and rinsed

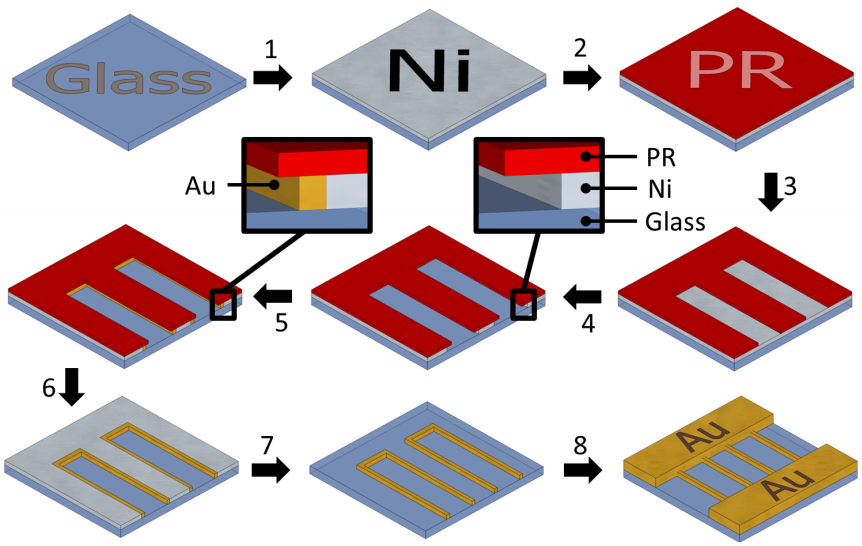

Figure 2.1: Process flow for the fabrication of thermophones consisting of an array of gold nanowires on glass using the Lithographically Patterned Nanowire Electrodeposition (LPNE) method.

with Millipore water (Mill-Q, $\rho > 18$ M$\Omega \cdot$ cm). The exposed nickel was etched in 0.80 M nitric acid for 6 min to produce horizontal trenches below the photoresist edges (4). Gold nanowires were then electrodeposited into the trenches (5) by immersing the patterned chip into commercial Au plating solution (Clean Earth Solutions™). This electrodeposition was potentiostatic at -0.90 V vs. saturated calomel electrode (SCE) using a Gamry Series G 300 potentiostat in conjunction with a one compartment three-electrode electrochemical cell with Pt foil as counter electrode. Deposition times of 4, 6, 10, and 12 minutes were used to create arrays with different nanowire widths. After electrodeposition of the gold nanowires, the photoresist and nickel working electrode were removed by acetone rinse (6) and etching in 0.80 M nitric acid (7) respectively. Finally, the nanowire array is protected by a 7 mm wide strip of paper while 10 nm of chromium and 200 nm of gold are thermally evaporated to form the contacts (8). The completed device, seen in Figure 2.2a, is an array of up to 4000 parallel gold nanowires with a pitch of 5 μm. The resistance of the arrays ranged from 9.5 to 92 Ω. The devices were characterized using an FEI Magellan XHR SEM (extreme high-resolution scanning electron microscope) at an accelerating voltage of 1 kV. No metals were sputtered onto the devices for imaging. Figure 2.3 shows SEM images of these polycrystalline

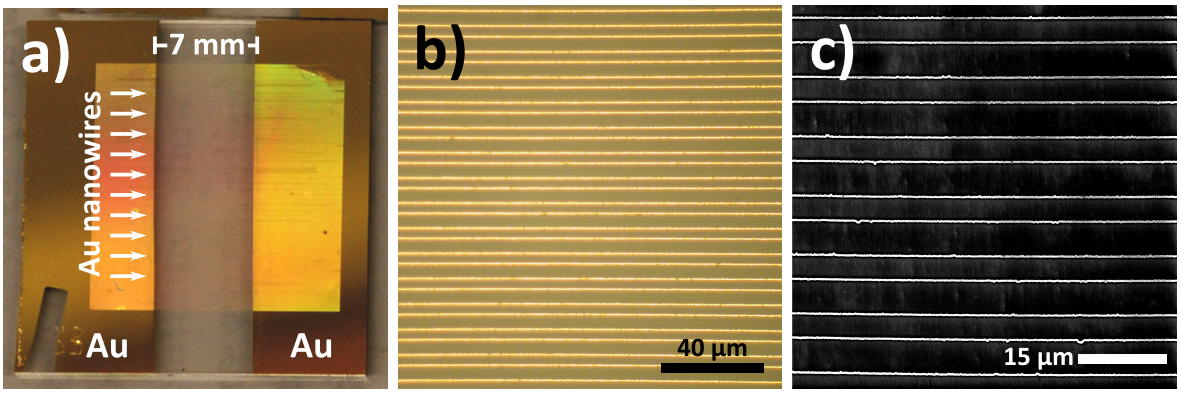

Figure 2.2: a) Optical image of the completed nanowire array on glass thermophone. b) Optical microscope image of the gold nanowire array. c) Scanning electron microscope image of the gold nanowire array.

nanowires produced the by four different electrodeposition times.

2.3 Acoustic Measurements

The experimental setup is shown in Figure 2.4. The driving ac signal was a sinusoidal wave generated by an HP 33120A function generator, which was then fed into a homemade amplifier based on the Texas Instruments LM1875T chip (see Appendix A). Two Keithley 2000 digital multimeters were used to measure the ac current and voltage being supplied to the nanowire devices. With the exception of the amplifier, all of the above equipment was controlled through a LabVIEW program to supply the desired electrical power input to the thermophones. The acoustic output was measured by an array of seven 0.125 inch Brüel & Kjær Type 4138 condenser microphones, paired with Type 2670 preamplifiers. The microphones were held at various angles by a hemicylindrical anechoic dome with an outer diameter of 12 inches. The dome interior was lined with 2 inch wedge-shaped acoustic foam (Foam Factory, Inc.). The microphones were positioned with their tips 3 cm from the center of the nanowire thermophone. The thermophone sits on the stage in the xy-plane, with the nanowires running parallel to the x-axis. The microphones occupy the zx-plane. For

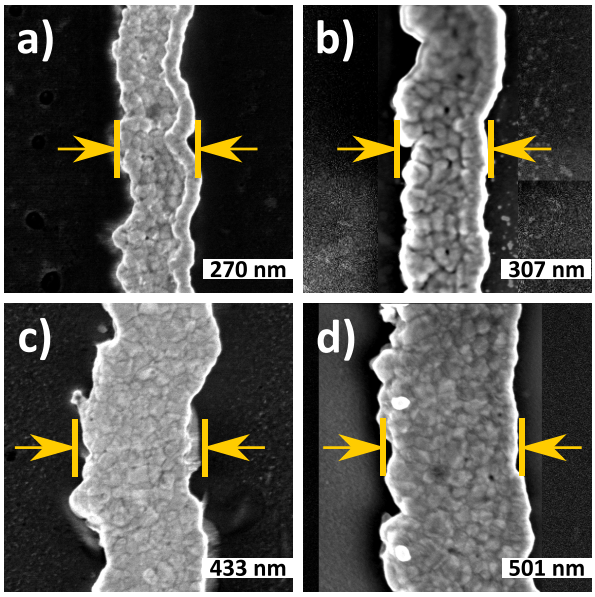

Figure 2.3: Scanning electron microscope images of gold nanowires showing the width range explored in this work. a) 270(±14) nm, b) 307(±21) nm, c) 433(±57) nm, and d) 501(±28) nm, where the values in parentheses are standard deviations. All nanowires were 100 nm in height.

each device, a background signal was first collected while no power was being supplied to the thermophone. This was later subtracted from the active signals. Correction factors for the microphones' actuator response (which accounts for the unique response profile of each microphone) and free-field response (which removes the interference of microphone with the sound field) were also applied. The measurements are also assumed to be in the acoustical far field. The boundary between the near and far field is typically approximated by the Rayleigh distance $R_0 = s/\lambda$, where s is the area of the sound source and λ is wavelength of sound[2]. R_0 is typically interpreted as the distance from the sound source where the pressure waves take on spherical characteristics, but it has been argued that far field behavior occurs much earlier at $R_0/4$, which fully contains the measurement range of this experiment [18].

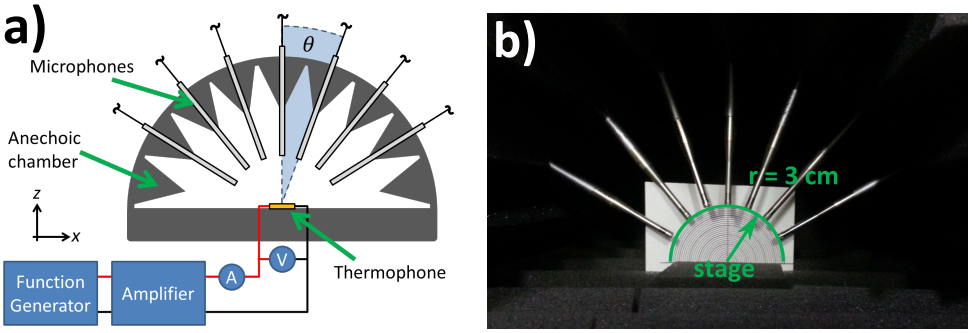

Figure 2.4: a) Diagram of the measurement setup. b) Optical image of the microphone array inside the anechoic dome with a calibration scale in place of the thermophone.

Chapter 3

Results and Discussion

3.1 Sound Emission and Efficiency

The sound pressure level as a function of output frequency generated by four nanowire arrays (from Figure 2.3) is shown in Figure 3.1. The SPL is defined as $20 \log_{10}(p/p_{ref})$, where p is the sound pressure and $p_{ref} = 20$ μPa. Despite varying the width of the nanowires, and therefore the heat capacity, by nearly a factor of two, no discernible performance difference was observed for these nanowire arrays.

The geometry of the thermophone, a fixed surface (the substrate) with a "vibrating" subsection (the heated air layer), is similar to that of a piston in a fixed baffle plate. Sound radiated into half-space from a baffled piston exhibits characteristic interference patterns in the off-axis sound pressure when the dimensions of the piston are large compared to the wavelength of sound.[2] These off-axis "nodes" are modeled by the directivity factor $D(\theta, \phi)$, which is the ratio of the sound pressure at some angle θ, ϕ to the on-axis pressure at the same distance from the sound source. For the case of a rectangular piston, $D(\theta, \phi)$ takes the

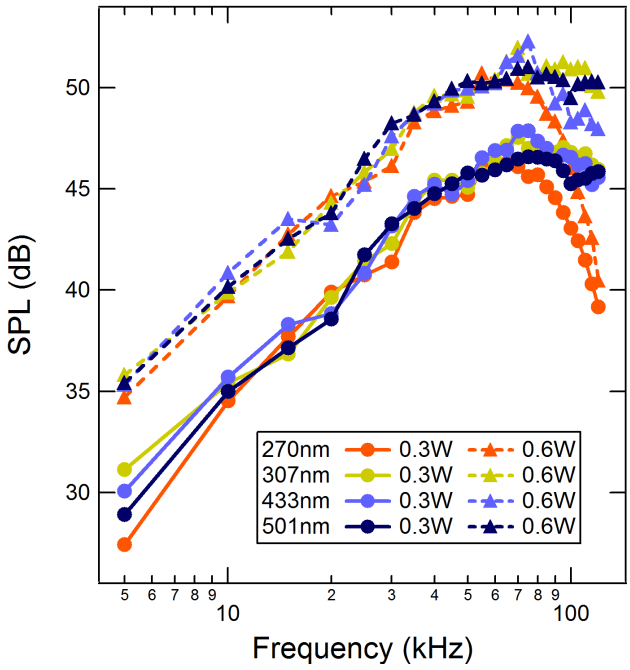

Figure 3.1: Sound pressure level vs. output frequency for nanowire arrays with input powers of 0.3 W (solid) and 0.6 W (dashed).

following form:[12]

$$D(\theta,\phi) = \text{sinc}\left(\frac{k_0 L_x}{2}\sin(\theta)\cos(\phi)\right)\text{sinc}\left(\frac{k_0 L_y}{2}\sin(\theta)\sin(\phi)\right) \tag{3.1}$$

where k_0 is the wavenumber $2\pi/\lambda$, and L_x and L_y are the dimensions of the piston surface. The microphones are defined to be in the $\phi = 0$ plane and their positions are described by θ, their angle with respect to the z-axis. Multiplying the on-axis pressure measurements, such as those in Figure 3.1, by the directivity factor produces an expected pressure amplitude at an angle θ. This is compared to the angular measurements of the 433 nm array in Figure 3.2.

Since the directivity factor does appear to give an accurate description of the sound pressure in all space, it can be used to estimate the total acoustical power output. The acoustical

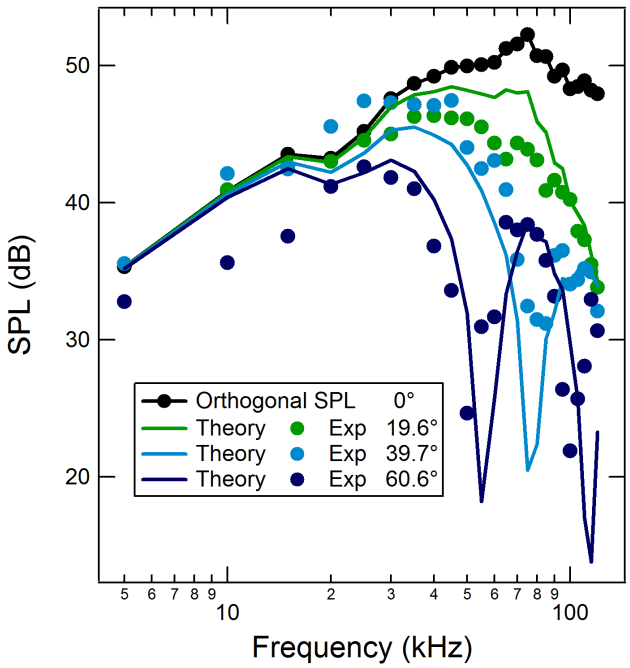

Figure 3.2: The off-axis SPL of a 100 nm (h) × 433 nm (w) nanowire array with $P_{in} = 0.6$ W. The measured SPL (dots) is compared to the expected level (lines) predicted by the directivity function $D(\theta, \phi)$ (Eq 3.1).

power P_{ac} is given by:[12]

$$P_{ac} = \frac{p_{rms}^2(r, \theta = 0) r^2}{\rho_0 c_0} \int_0^{2\pi} \int_0^{\pi/2} D^2(\theta, \phi) \sin\theta d\theta d\phi \tag{3.2}$$

where $p_{rms}(r, \theta = 0)$ is the measured on-axis pressure at a distance of r from the device, and ρ_0 and c_0 are respectively the density and speed of sound in air at 25°C and 1 atm. Dividing this value by the electrical input power, we arrive at the efficiency values shown in Figure 3.3. The highest efficiency observed in this study, 1.9×10^{-10}, was achieved by a 515 nm array at 25 kHz with an input power of 2.5 W (Figure 3.5c). A general trend observed across the data of Figure 3.3a is that of increasing efficiency with increasing input power. This correlation is expected since the system can be considered a heat engine following Carnot efficiency limit of $\eta \leq 1 - \frac{T_C}{T_H}$, where T_H is the temperature of the heat reservoir (nanowires) and T_C is the

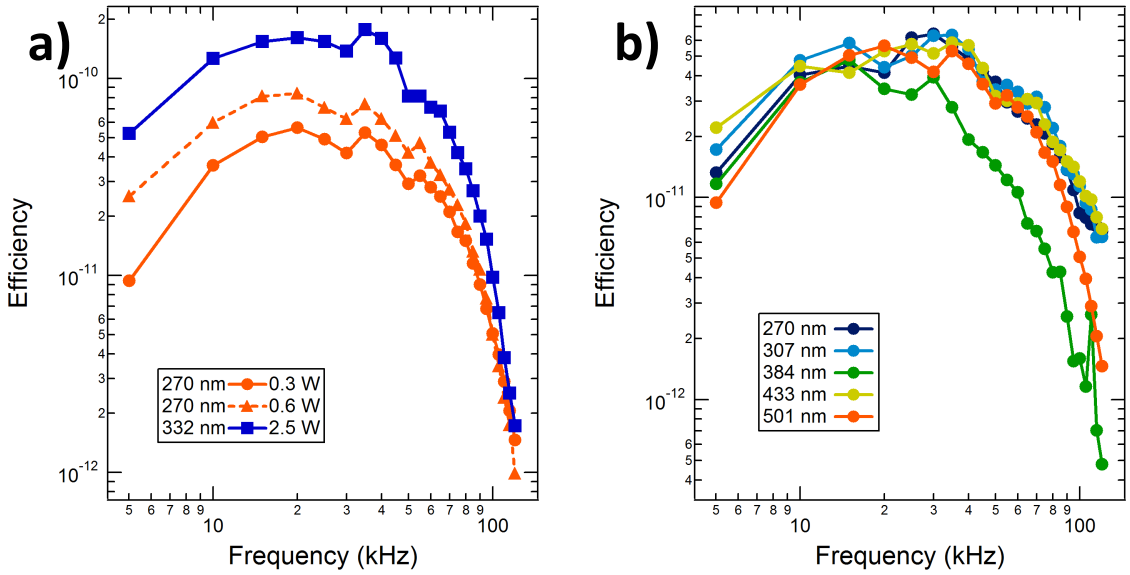

Figure 3.3: Plots of the efficiency as a function of frequency. a) Comparison of power-dependance for 0.3 W, 0.6 W, and 2.5 W. b) Comparison of four wire widths as indicated at $P_{in} = 0.3$ W. All nanowires were 100 nm in height.

temperature of the cold reservoir (atmosphere). Since the different nanowire arrays produced remarkably similar SPL, it is not surprising that they also display very similar efficiencies across the measured frequency spectrum (Figure 3.3b).

3.2 Modeling Sound Emission

The original work of Arnold and Crandall[1] readily explains why an array of nanowires behaves like a metal film in terms of the thermoacoustic response. They surmised[1] that the cyclic heating of a boundary layer of air at the conductor surface generates pressure waves. They further hypothesized that the heated boundary layer could be modeled as a piston in place of the thermophone, and this hypothesis was supported by measurements of a thin Pt foil thermophone.[1] The radius of the heated boundary layer is defined to be one thermal wavelength, $\lambda_T = 2(\pi\alpha/f)^{1/2}$, from the conductor surface, where f is the frequency of thermal wave and α is the thermal diffusivity of air. For nanowires, this region

is approximated as a hemicylinder with a radius between 49 μm at 120 kHz and 238 μm at 5 kHz around each nanowire. Given that the nanowire array has a pitch of just 5 μm, the heated boundary layers from adjacent nanowires are overlapped. The result is that planar pressure waves are produced by the nanowire array in the acoustical near field, mimicking the behavior of metal film-based thermophones.

Improvements to this theory were later made by Xiao *et al.* [16] to more accurately describe the sound produced by an ultra-low heat capacity conductor like the CNT films in their study. Their expression for the root mean square pressure in the far field, p_{rms}, is:

$$p_{rms} = \frac{\alpha^{1/2}\rho_0}{2\pi^{1/2}T_0}\frac{P_{in}}{r}\frac{f^{1/2}}{C_s}\frac{f/f_2}{\left[\left(1+(f/f_1)^{1/2}\right)^2+\left(f/f_2+(f/f_1)^{1/2}\right)^2\right]^{1/2}} \tag{3.3}$$

where $f_1 = \alpha\beta_0^2/\pi\kappa^2$ and $f_2 = \beta_0/\pi C_s$. Here, α, ρ_0, κ, and T_0 are the thermal diffusivity, density, thermal conductivity, and temperature of the ambient gas. P_{in} is the input power, and C_s is the heat capacity per unit area of the conductor. Finally, β_0 is the heat loss per unit area of the conductor per unit temperature above T_0. In applying this analytical model to the data, β_0 was used as a fitting parameter. The plateau region in the SPL ($f > 70$ kHz), which is not predicted by the model, was excluded from the fitting calculation. Such plateaus at high frequencies are characteristic of thermophones and were first observed by Shinoda *et al.*[7]. This change in behavior usually attributed to near field interference [17] or heterogeneous substrates, whether in the form of multiple layers [7, 11, 8] or air domains [13], but neither of these are present in our thermophone.

The resulting curve derived from Eq 3.3 (Figure 3.4, orange traces) fits our data poorly. Presumably, this is because the derivation of Eq 3.3 assumes the presence of air on both sides of the surfaces of the conductor, whereas the nanowire arrays of interest here are

supported on glass. This problem was solved by Vesterinen *et al.* who accounted for the effect of a substrate on the thermophone performance, redefining f_2 as:[12]

$$f_2 = \frac{\beta_0}{2\pi C_{s,sub}} = \frac{\beta_0}{2\pi C_{sub}} \left(\frac{f}{\pi \alpha_{sub}} \right)^{1/2} \tag{3.4}$$

where C_{sub} and α_{sub} are the heat capacity and thermal diffusivity of the substrate. Once again using β_0 as a fitting parameter, the resulting curve (Figure 3.4, blue traces) provides a much improved approximation of our data. The values of β_0 recovered from these fits are 2.1×10^5 W/(m^2·K) and 2.5×10^5 W/(m^2·K) for 0.3 W and 0.6 W, respectively. By comparison, a freestanding single-layer carbon nanotube film was reported to have a significantly lower β_0 of 28.9 W/(m^2·K)[16], and β_0 has previously been shown to increase as a function of input power[17] as seen here. Efficient diffusive transfer of heat by nanowires into the glass surface is expected based upon the hemicylindrical heat diffusion field in the glass that is dictated by the nanowire geometry.[3] Anecdotally, device "overheating" proved to be problematic for input powers of 2.5 W which sometime induced burning of the foam stage; for several devices, increasing the input power rapidly caused the glass substrate to shatter (see Appendix B for images). Since β_0 was determined as an adjustable parameter, it cannot be said with certainty how much these values represent the true losses in the system and how much they represent an incomplete description of the thermoacoustic effect. The choice of less thermally conductive substrates,[8, 10] and the suspension of the conductor in air,[12, 13] have been shown to improve thermophone performance (Table 1.1). Hu *et al.* [4] also developed an analytical model for thermophone behavior that accounts for the substrate's properties, although it ignores the properties of the conductor. Their expression for the root mean

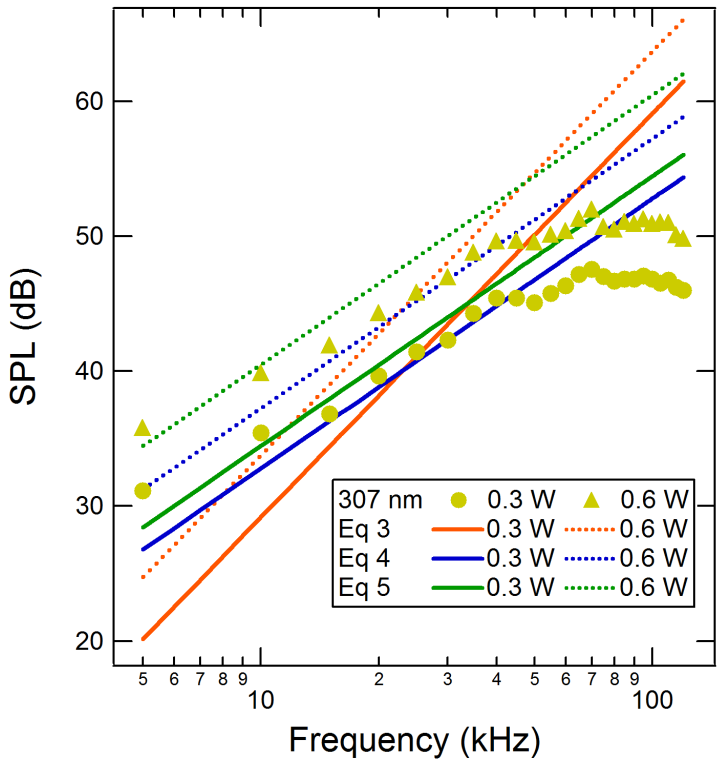

Figure 3.4: The analytical model described by Eq 3.3 (orange) and with the correction from Eq 4 (blue), both fitted to measurements from a 100 nm (h) × 307 nm (w) nanowire array. The model of Hu *et al.* [4] (Eq 3.5) is shown in green.

square pressure, translated into the far field, is

$$p_{rms} = \frac{R_0}{\sqrt{2}r}\frac{\gamma - 1}{v_g}\frac{e_g}{e_s + e_g}q_0 \tag{3.5}$$

where γ is the heat capacity ratio of air, v_g is the speed of sound in air, and e_g and e_s are the thermal effusivity of air and the substrate. The resulting curve is also shown in Figure 3.4. This model consistently overestimates the pressure amplitude generated by the thermophone, and the deviation seems to increase as a function of input power.

Table 3.1: Value of the fitting parameter, β_0, in the calculations of Figure 3.5

f (kHz)	β_0 (10^5 W/m^2·K)[a]
5	1.25
10	1.56
25	1.59
50	2.30
100	3.69

[a] β_0 is the heat loss per unit area of the conductor per unit temperature above a reference temperature, T_0.

3.3 Effects of Input Power

Figure 3.5 shows the performance of a 515 nm thermophone while increasing the input power from 0.5 W to 2.5 W. The curves shown are best fits using the correction above with the fit parameters shown in Table 3.1. For reference, the value of β_0 for SPL vs. frequency at 2.5 W for this device is 2.3×10^5 (MW/m^2·K), similar to those seen as a function of power. Looking at sound pressure vs. power in Figure 3.5a, the expected linear relationship from Eq 3.3 holds by and large, although some deviation is seen at the highest powers and frequencies. This linear relationship has also been observed in several studies [11, 10, 8, 9, 13] for $f \leq$50 kHz and lower input powers of $P_{in} \leq$1.5 W. The PEDOT thermophone[9] was measured at similar input power densities (W/cm^2) to those shown in this study, but the data was presented without a linear fit and cannot be conclusively compared to our data. Figure 3.5c shows the relationship between power, frequency, and efficiency for gold nanowire thermophones. As seen in Figure 3.3, the device efficiency increases with input power. Of these five frequencies measured, 25 kHz is produced most efficiently.

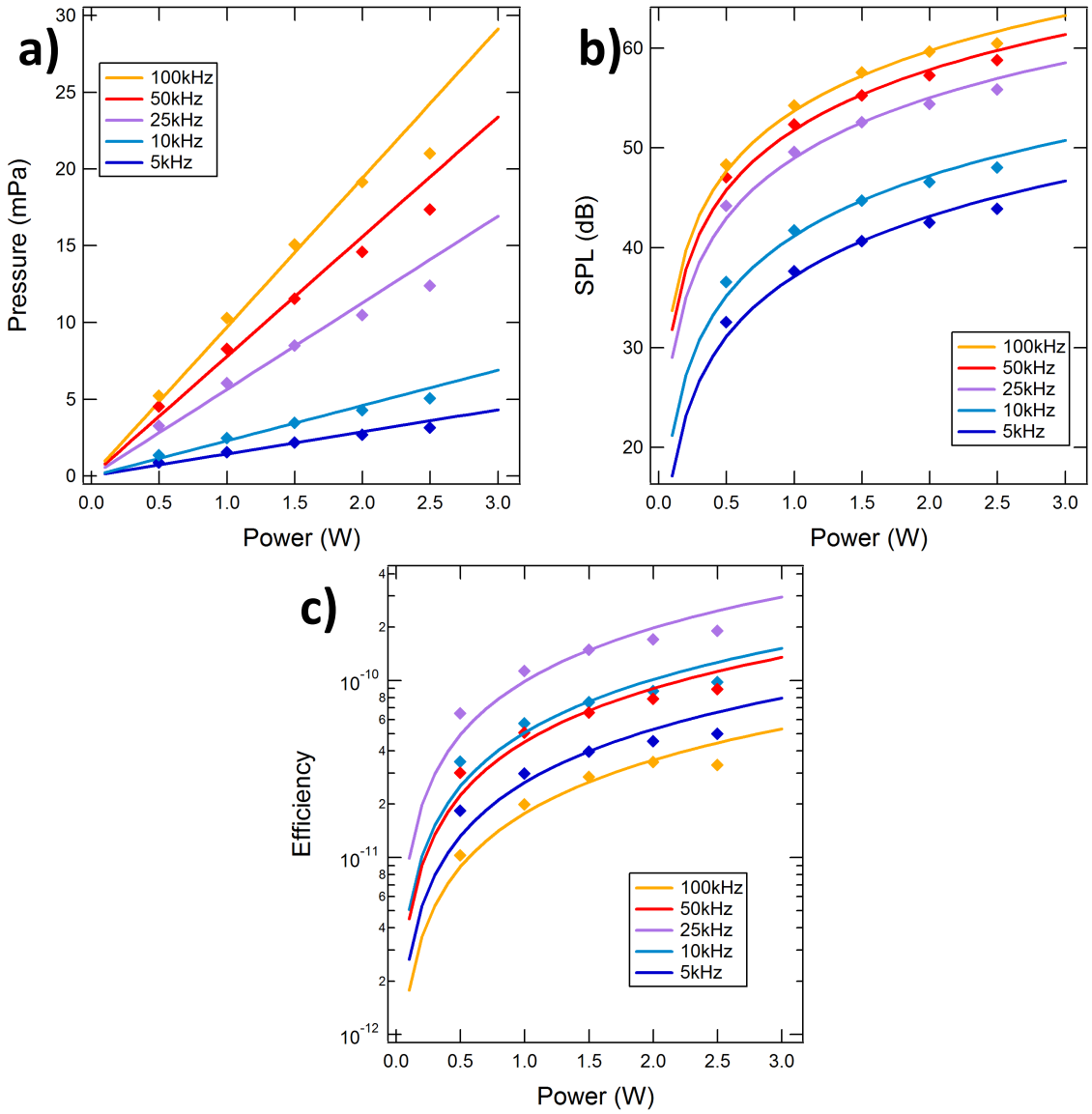

Figure 3.5: Comparison of theory for metal film thermophones with experimental data for a gold nanowire array (100 nm (h) × 512 nm (w)): a) Sound pressure, b) sound pressure level (SPL), and, c) efficiency as a function of input power. These data are presented at five frequencies as indicated. Solid curves are fits of Eq 4 to the experimental data. Parameters corresponding to the best fits are summarized in Table 3.1.

Chapter 4

Conclusion

In this initial investigation of metal nanowire thermophones involving arrays of long (mm scale), noninteracting gold wires, the conclusion is that these nanowire arrays behave much like metal films in terms of their ability to produce sound using the thermoacoustic effect. In fact, in spite of the dramatically lower coverage of the glass surface by gold, θ_{Au}, which for the nanowire arrays investigated here is $0.054 < \theta_{Au} < 0.1$ depending upon the nanowire width, the properties of these nanowire arrays are accurately predicted by equations derived for metal film thermophones where $\theta_{Au} = 1.0$. Remarkably, even nuances such as angular "nodes" for the off-axis SPL versus frequency data, predicted by the directivity factor, are faithfully reproduced by these nanowire arrays. These nanowire arrays mimic the thermoacoustic behavior of metal films because the thermal wavelength, λ_T, at the surface of each nanowire is much larger than the distance between them, so the nanowire array generates a plane wave in the near field just like a film.

A lower efficiency for sound production is obtained from nanowires as compared with metal films (Table 1.1), likely reflecting the more efficient dissipation of the Joule heat in nanowires by hemicylindrical, rather than planar, diffusion from the nanowire into the glass surface.[3]

This picture is supported by the large values of β_0, exceeding 10^5 W/(m^{2}K), that we calculate for the nanowire arrays investigated in this study. Based upon this hypothesis, for metal nanowires systems where suspension of the nanowires away from the surface is possible, a dramatically elevated efficiency can be expected.

Bibliography

[1] H. Arnold and I. Crandall. The thermophone as a precision source of sound. *Physical Review*, 10(1):22–38, 1917.

[2] D. Blackstock. Fundamentals of physical acoustics. *Wiley-Interscience*, pages 440–465, 2000.

[3] H. S. Carslaw and J. C. Jaeger. Conduction of heat in solids. *Oxford: Clarendon Press, 1959, 2nd ed.*, 1, 1959.

[4] H. Hu, T. Zhu, and J. Xu. Model for Thermoacoustic Emission from Solids. *Appl. Phys. Lett.*, 96(21):214101, 2010.

[5] E. J. Menke, M. A. Thompson, C. Xiang, L. C. Yang, and R. M. Penner. Lithographically Patterned Nanowire Electrodeposition. *Nat. Mater.*, 5(11):914–9, Nov. 2006.

[6] A. O. Niskanen, J. Hassel, M. Tikander, P. Maijala, L. Grönberg, and P. Helistö. Suspended Metal Wire Array as a Thermoacoustic Sound Source. *Appl. Phys. Lett.*, 95(16):163102, 2009.

[7] H. Shinoda, T. Nakajima, K. Ueno, and N. Koshida. Thermally Induced Ultrasonic Emission from Porous Silicon. *Nature*, 400(August):853–855, 1999.

[8] H. Tian, T.-L. Ren, D. Xie, Y.-F. Wang, C.-J. Zhou, T.-T. Feng, D. Fu, Y. Yang, P.-G. Peng, and L.-G. Wang. Graphene-on-Paper Sound Source. *ACS Nano*, 5(6):4878–4885, 2011.

[9] H. Tian, D. Xie, Y. Yang, T.-L. Ren, T.-T. Feng, Y.-F. Wang, C.-J. Zhou, P.-G. Peng, L.-G. Wang, and L.-T. Liu. Poly(3,4-ethylenedioxythiophene):poly(styrenesulfonate)-Based Organic, Ultrathin, and Transparent Sound-Emitting Device. *Appl. Phys. Lett.*, 99(23):233503, 2011.

[10] H. Tian, D. Xie, Y. Yang, T.-L. Ren, Y.-X. Lin, Y. Chen, Y.-F. Wang, C.-J. Zhou, P.-G. Peng, L.-G. Wang, and L.-T. Liu. Flexible, Ultrathin, and Transparent Sound-Emitting Devices Using Silver Nanowires Film. *Appl. Phys. Lett.*, 99(25):253507, 2011.

[11] H. Tian, D. Xie, Y. Yang, T.-L. Ren, Y.-F. Wang, C.-J. Zhou, P.-G. Peng, L.-G. Wang, and L.-T. Liu. Transparent, Flexible, Ultrathin Sound Source Devices Using Indium Tin Oxide Films. *Appl. Phys. Lett.*, 99(4):043503, 2011.

[12] V. Vesterinen, A. O. Niskanen, J. Hassel, and P. Helisto. Fundamental Efficiency of Nanothermophones: Modeling and Experiments. *Nano Lett.*, 10(12):5020–5024, Nov. 2010.

[13] Y. Wei, X. Lin, K. Jiang, P. Liu, Q. Li, and S. Fan. Thermoacoustic Chips with Carbon Nanotube Thin Yarn Arrays. *Nano Lett.*, 13(10):4795–801, Oct. 2013.

[14] C. Xiang, S.-C. Kung, D. K. Taggart, F. Yang, M. A. Thompson, A. G. Gu, Y. Yang, and R. M. Penner. Lithographically Patterned Nanowire Patterning Electrically Continuous Metal Nanowires on Dielectrics. *ACS Nano*, 2(9):1939–1949, 2008.

[15] C. Xiang, Y. Yang, and R. M. Penner. Cheating the Diffraction Limit: Electrodeposited Nanowires Patterned by Photolithography. *Chem. Commun.*, (8):859–73, 2009.

[16] L. Xiao, Z. Chen, C. Feng, L. Liu, Z.-Q. Bai, Y. Wang, L. Qian, Y. Zhang, Q. Li, K. Jiang, and S. Fan. Flexible, Stretchable, Transparent Carbon Nanotube Thin Film Loudspeakers. *Nano Lett.*, 8(12):4539–45, Dec. 2008.

[17] L. Xiao, P. Liu, L. Liu, Q. Li, Z. Feng, S. Fan, and K. Jiang. High Frequency Response of Carbon Nanotube Thin Film Speaker in Gases. *J. Appl. Phys.*, 110(8):084311, 2011.

[18] J. Zemanek. Beam behavior within the nearfield of a vibrating piston. *J. Acoust. Soc. Am.*, 49(1B):181–191, 1971.

Appendix A

Amplifier Design

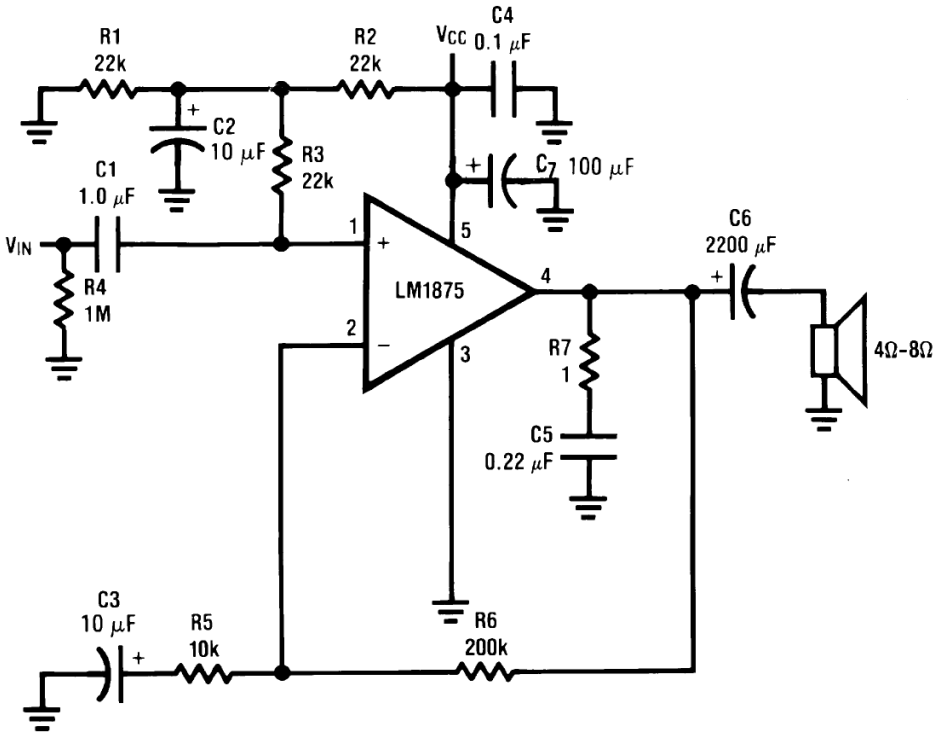

Figure A.1: Circuit diagram for the amplifier used in this experiment provided by Texas Instruments: http://www.ti.com.cn/cn/lit/ds/symlink/lm1875.pdf

Appendix B

Substrate Overheating

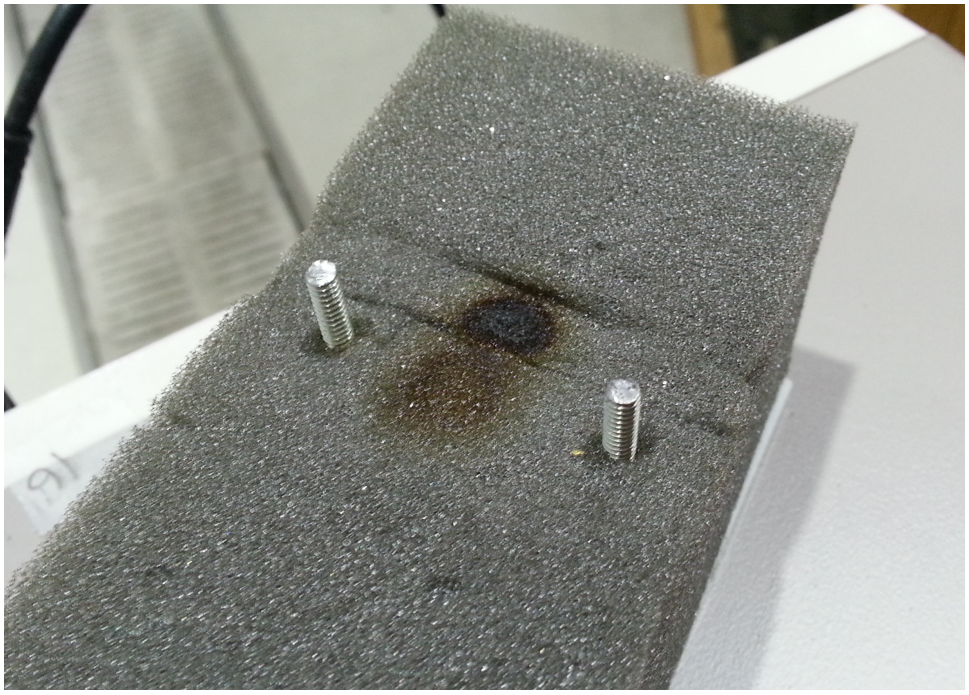

Figure B.1: Burn marks on the sample stage after running several gold nanowire thermophones at $P_{in} = 2.5$ W.

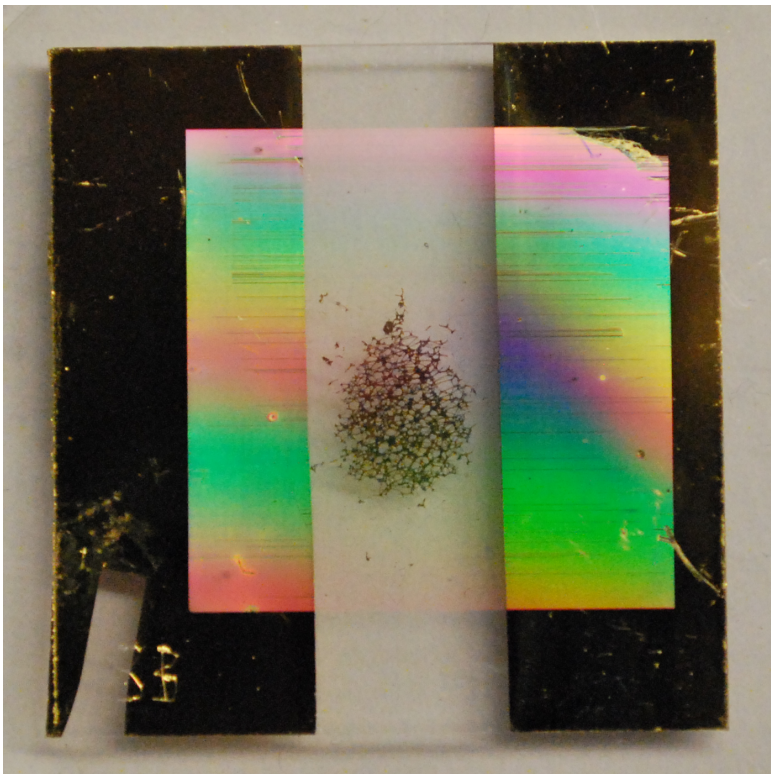

Figure B.2: Optical image of a gold nanowire thermophone after 2.5 W operation. Note the dark spot at the center, where acoustical foam has adhered to the back of the slide due to high temperatures in the glass substrate.

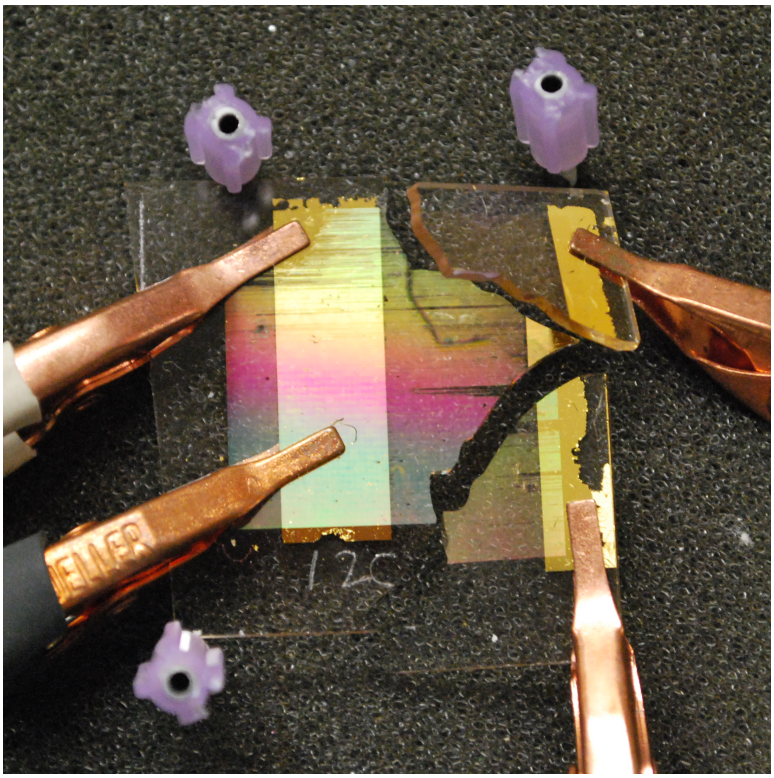

Figure B.3: Optical image of a shattered gold nanowire thermophone. Increasing the input power too quickly would often cause this.

Appendix C

Constants Used in Calculation

Table C.1: Parameters used in calculations

Variable	Parameter	Value
κ	thermal conductivity of air	2.63×10^{-2} W/m K
ρ_0	density of air	1.16 kg/m^3
α	thermal diffusivity of air	2.25×10^{-5} m^2/s
T_0	temperature of air	300 K
C_s	heat capacity per unit area	$\rho_{Au} v_{nw} C_{Au} N/A$
ρ_{Au}	density of gold	1.93×10^4 kg/m^3
C_{Au}	heat capacity of gold	129.1 J/kg K
v_{nw}	volume of a single nanowire	7 mm $\times$ 100 nm $\times w$
N	number of nanowires	4000 wires
A	thermophone area	1.4×10^{-4} m^2
α_{sub}	thermal diffusivity of glass	4.69×10^{-7} m^2/s
C_{sub}	heat capacity of glass	705 J/kg K
γ	heat capacity ratio of air	1.4
v_g	speed of sound in air	343.2 m/s
e_s	thermal effusivity of glass	$\sqrt{\kappa_s \rho_s C_{sub}}$
κ_s	thermal conductivity of glass	0.86 W/m K
ρ_s	density of glass	2.6×10^3 kg/m^3
e_g	thermal effusivity of air	$\sqrt{\kappa \rho_0 C_g}$
C_g	heat capacity of air	1007 J/kg K